Numerical Investigation on Shock Train Control and Applications in a Scramjet Engine

Fei Xing, Can Ruan, Yue Huang, Xiaoyuan Fang

School of Aerospace Engineering, Xiamen University, Xiamen 361005, PR China

and

Yufeng Yao

Department of Engineering Design and Mathematics, University of the West of England, Bristol BS16 1QY, UK

Abstract

Different factors which help to control the shock train in the scramjet isolator and combustor were analyzed via numerical investigations, and were applied to a whole scramjet engine in the working environment. A streamline traced Busemann inlet is proposed and simulated along with an isolator. During the combustor design, the influence of boundary layer thickness, slot bleeding, cavity and hydrogen injection position on the basic combustor performance with uniform inlet flow condition are investigated, and it was found that the boundary layer bleeding could prevent the shock train from moving upstream, and the cavity could further enhance the combustion efficiency. By arranging hydrogen injections at certain intervals, it could reduce the combustion back pressure. An improved basic model by integrating the aforementioned advantages is then numerically studied. The results have shown that the improved combustor model contained a section of shock train which can reduce the loads on the isolator. Another model with bleeding slots in the isolator is also found able to raise the maximum chemical equivalence ratio from 0.7 to 1, but unfortunately it comes with undesirable combustion efficiency decrease.

Nomenclature

Ma   Mach number

P   static pressure Pa

T   static temperature Pa

U   stream wise velocity m/s

H   flight height m

$y+$ y-coordinate in wall unit

δ boundary layer thickness

y   the distance from the wall mm

γ   the ratio of specific heats

Pr   Prandtl number

η   combustion efficiency

σ   total pressure recovery coefficient

ϕ   the chemical equivalence ratio

Subscripts

1   location 1 at the entrance of inlet

2   location 2 at the cowl lip of inlet

3   location 3 at the exit of inlet

∞   freestream

W   parameters on the wall

1. **Introduction**

In order to avoid carrying a large amount of on-board oxidizer, hypersonic flight vehicle design was the development and application of supersonic combustion ramjet (scramjet), a variant of air-breathing ramjet jet engine, in which combustion takes place at supersonic airflow speed [1].

There are several advantages of applying this engine type; e.g. lower static temperature and pressure even after the diffuser where the flow remains at supersonic speed, reduction of dissociation problems as the gases being expanded in the engine exhaust, and further reduced diffuser losses, etc. However, high flow velocity inside the scramjet combustion chamber often poses great challenges for the air/fuel mixing and the combustion progress within desirable length scales, due to complex shock-shock, shock/boundary-layer and shock-flame interactions. At the same time, when the flame is held in the combustor, because the combustor working back pressure increases and moves upstream of the shock wave of isolator that can cause the inlet 'unstart'. Hence it is very important for researchers and designers to consider the scramjet engine as an integrate component, instead of several separated parts.

Flame holding is another challenging issue in designing a scramjet engine, as a stable flame-holding system for a wide range of operating conditions is critical to engine performance. Various flame-holding techniques have been developed for supersonic combustors and their features were reviewed in reference paper [2]. Cavity-based flame holder, as an integrated fuel injection/flame-holding approach, has recently been attracted considerable attentions due to its characteristics of lower total pressure loss and better fuel/air mixing enhancement. Because the drag associated with flow separation is much less over a cavity than that for a bluff-body, a small-size cavity inside a combustor makes it suitable to be a stable flame holder with relatively little total pressure drop. Several control methods have been proposed to suppress the flow oscillations in a cavity. Among

them, a cavity with an angled rear wall was devised to suppress the unsteady nature of the free shear layer by eliminating the generation of traveling waves inside the cavity [2] and [3].

Most studies of cavity-based flame-holder have been done numerically without considering the chemical reaction and the experimental tests [4], [5], [6] and [7]. However, for a practical application to a supersonic combustion, it is crucial and highly demanding to carry out a numerical analysis on a cavity flow for flame holding in chemical reactions, prior to expensive experiments. In this paper, the simulation is conducted under the whole engine environment and the chemical reaction of the hydrogen fuel is also taken into consideration when calculating the combustion performance of the engine.

Shock train controlling is another challenging issue to be researched in this paper. In order to generate more thrust from a scramjet engine, more heat will be needed in the combustor, which would effectively raise the pressure and the temperature of airstream and enhance the thrust ultimately [8]. This process is seemingly acceptable for the flow field downstream of the combustor. However, exorbitant pressure in the combustor will have a significant side effect on the flow field upstream of the combustor, such as the interaction between the shock-wave and the boundary layer in the isolator may result in strong adverse pressure gradient and flow separation that will form strong reflected shock waves and even shock trains, the shock trains can propagate upstream far enough towards the inlet and would disrupt the inflow property. This will result in possible inlet unstart, due to the sharp decrease of air mass flow captured compared with normal operation conditions [9], [10] and [11].

There have been many investigations into the topic of shock train in the scramjet to prevent possible unstart problem. Zinnecker [12] tested A series of physics-based isolator models which were constructed through spatial discretization of the two-dimensional and one-dimensional Euler equations, two disturbance rejection controllers were designed and both controllers were found to maintain the shock wave within 3cm (26.1% of the duct height) of the specified location. By raising a mechanical flap located downstream of the isolator, unstart was triggered in experiments [13] and [14]. Do et al. [15] investigated the unstart phenomena initiated by jet injection downstream of an inlet/isolator in a Mach 5 wind-tunnel.

From above we can conclude that the system parameters including the geometrical and working conditions may affect greatly of the shock train characters and unstart phenomenon. In this paper, the boundary layer thickness accompanied by the slot bleeding technology were studied to investigate how the boundary layer affect the combustion performance and back pressure in the combustor, at the same time different hydrogen injection plans have been proposed and discussed to investigate its influence on the shock train generation and unstart issue. After this, three-dimensional scramjet model with a truncated Busemann inlet presented in reference 16 will be investigated by via a computational fluid dynamics (CFD) solution based on solving Reynolds-averaged Navier-Stokes (RANS) equations with turbulence and combustion models. Both turbulence and combustion model assessments will be carried out and comparisons of surface pressure distributions with the experimental data will be made. In particular, numerical cases for bleeding slot combined with cavity will be analyzed in a systematic manner and CFD predicted parameters, such as static pressure, temperature, fuel concentration and heat release, will be compared. The primary goal of the present research is to investigate and compare the feasibility and the effectiveness of

different methods in controlling the shock trains from moving further upstream of the combustor, and also the effect of the shock trains affecting the progress of the combustion, thus to assess the applicability of the configuration including the whole scramjet engine performance for the high-speed scramjet applications.

2. **Model Configuration and Numerical Approach**

2.1. Model Configuration and Meshing

In particular, the inlet design is taken in three steps: truncation, streamline-traced and renewing the cowl. In this study, a full Busemann inlet is firstly developed by solving the Taylor–Maccoll equation [16] and [17] with a MATLAB program. The original full Busemann inlet is shown in Fig. 1(a), it has been designed for the conditions of incoming Mach number M∞ = 6 at the entrance and the truncation wedge angle of the leading-edge is 3°.
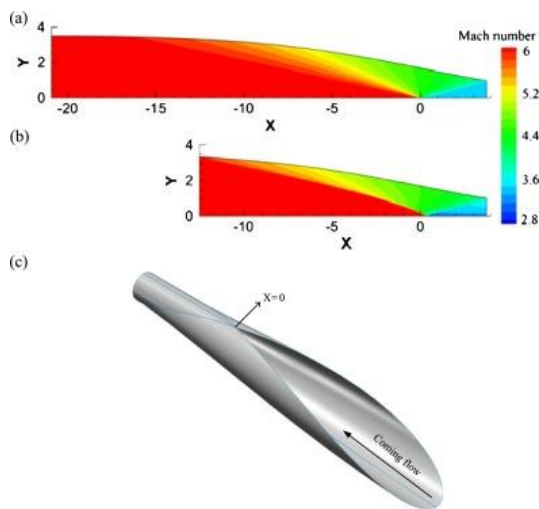
Fig. 1. Ma contours of (a) the full Busemann inlet; (b) the truncated Busemann inlet; (c) 3D model of truncated Busemann inlet.

The Busemann inlet design will result in smaller wetted areas, compared to that of normal inlet design, to reduce internal drag, and lower heating load to the structure [6], [7], [8] and [9], which would yield a further reduction in the amount of active cooling airflow required by a similar two-dimensional geometry. However, the full-scale streamline-traced Busemann inlet would be too long to achieve the lower total pressure loss under the assumption of inviscid flow. In order to meet the restriction of overall weight and size limits of the scramjet, the inlet configuration should be truncated without severe deterioration in terms of aerodynamic performance and efficiency.

As for truncation, from Fig. 1 (a) we can see that a shock is generated and reflects at x=0mm, when x is lower than ~−13 mm, the flow field changes slightly, which means we can truncate the cowl to decrease the length of the inlet while obtaining the flow field similar with the full inlet. A truncated version of the full Busemann inlet is proposed and the configuration (i.e. the points of the internal conical flow field) is obtained, the Ma contour of truncated inlet is shown in Fig. 1(b) and Fig. 1(c) illustrates the 3D model of truncated Busemann inlet. The truncation of the original Busemann inlet

geometry will reduce the inlet length remarkably hence causing the performance decrease, but still within an acceptable range according to the published papers [18] and [19]. For example, using a truncated length of 2/3 of the full Busemann inlet length, the inviscid total pressure recovery can still maintain up to 89.6%.

On the other hand, from Fig. 1(b) we can see that the shock reflection point of truncated inlet relocates at x>0 but not X=0 shown in Fig. 1(a) for full Busemann inlet, which makes it worthy to renew the edge of the cowl of the inlet to increase the thrust-weight ratio of the whole engine. The process of renewing the cowl is shown in Fig. 2, Fig. 2(a) give a 3D schematic of the truncated inlet, the pale blue area is used to represent the surface of the shock, which is also shown in Fig. 1(b). The edge of cowl is then rearranged as shown in Fig. 2(b), the location of the new edge is determined based on the shock reflection area shown in Fig. 1(b) and Fig. 2(a). Until now, the final geometrical model of the Busemann inlet is determined as shown in Fig. 2(b).
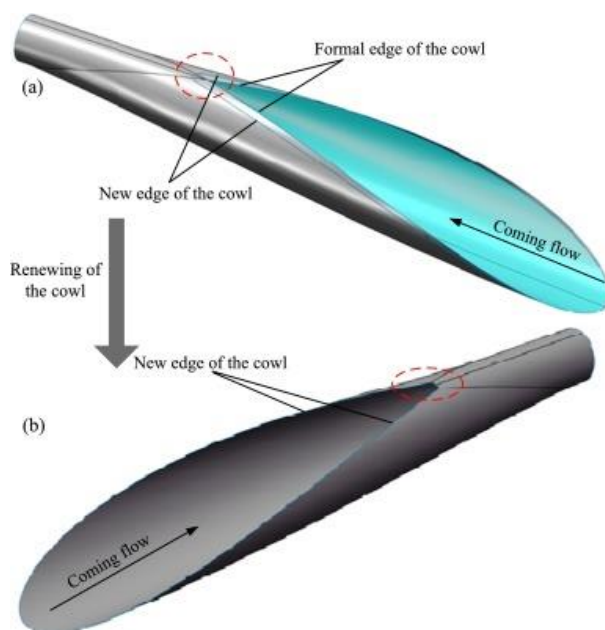

Fig. 2. Schematic of inlet truncation: a 3D view.

Depending on the geometric model, either structured or unstructured computational grids will be generated; i.e. structured grid for the cases without the inlet, and unstructured grids for the cases with the inlet (because of the specific streamline tracing shape of the inlet, structured grid was highly distorted with poor quality thus not used). The mesh is generated by using the commercial software ICEM. The initial spacing of the boundary layer mesh in all cases was 5×10^{-3} mm, which results in y+ values less than 1 over the majority of the wall surfaces, and the total grid nodes are about 1 million. Fig. 3 shows one of the mixed tetra and hex meshes used for calculations.
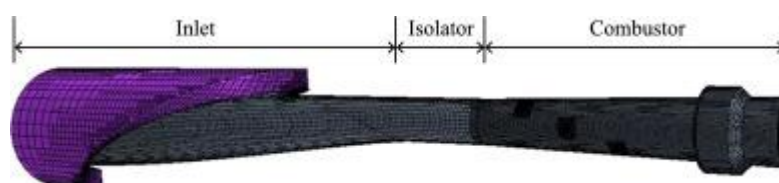
Fig. 3. An example of tetra-hex mesh of complete computational domain.

2.2. Computational Setup

A commercial CFD software ANSYS-FLUENT is applied. This software contains various sub-models to simulate supersonic flow phenomena. Several key elements will be explored to realize the capabilities of the software in simulating shock-wave/boundary-layer and shock-shock interactions, gas combustion, along with mass, momentum and heat transfer transport characteristics in the supersonic airflow.

Some popular turbulence models such as k–ε model and Shear-Stress-Transport (SST) model are considered for assessing their capability for the cases with strong shock-wave/boundary-layer interactions that may cause possible flow separation and also shock-induced-combustion phenomena. The good agreements of using the SST model to predict the supersonic flow in the configurations such as inlets and isolators have been obtained by many other researchers as saw in reference papers [20], [21], [22], [23] and [24] recently. In section 3, the numbers of structured grid points for the cases are around 0.5 million and in section 4, the grid nodes are about 1 million, y plus of all the cases is under 10.

The simulations were performed using the k–ω SST two-equation eddy viscosity model coupled with Eddy-Dissipation Model (EDM) to simulate turbulent flow and combustion. The Eddy Dissipation Model (EDM) assumes the combustion chemical reaction is infinitely fast, hence the fuel consumption in the turbulent diffusion flame will be solely determined by the mixing rate of fuel and oxidizer, and this rate is inversely proportional to the turbulence time scale (i.e. turbulent kinetic energy divided by turbulent dissipation). All cases were run using FLUENT's coupled, density-based, implicit solver.

The numerical results were based on steady-state solutions. For the cases with the inlet, the flow conditions for these models are air at 23.3% of oxygen and 76.7% of nitrogen in terms of mass fraction, flight height H=24 km, flight Mach number M∞=6, static pressure p∞=2930.7 Pa, static temperature T∞=220.7 K, respectively. In the cases without the inlet, the airstream conditions are Mach number Ma_3=3.23, static pressure p_3=41.3 kPa, static temperature T_3=586.7 K, respectively. All these values are mass weighted average parameters at the exit of the inlet.

2.3. Simulation Model and Mesh Evaluation

In the present study, results from steady CFD simulations are going to compare with the experimental data of Zheng [25] on supersonic combustion fueled hydrogen tests. The combustion model is used in reference paper [25] is shown in Figure 4. The isolator length is 200m and height is 18 mm. The total length of combustor is 300 mm, and the expansion angle of the upper wall is 3° starting at 80 mm from the combustor inlet, while the lower wall is flat. The height of the dump is 3 mm, same for both upper and lower walls, which connects with the isolator and the combustor. The fuel injection hole is introduced at a location 95 mm from the inlet of the combustor, and the diameter is 1.2 mm. Hydrogen gas is fueled from 7 equally spaced holes and the chemical equivalence ratio is controlled by opening and/or closing theses injection holes.
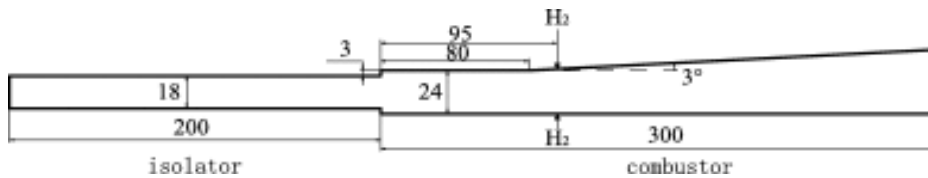
Fig. 4. A dual model ramjet combustor model in mm (Ref. [25]).

As the geometry is symmetric and the flow is primarily in axial manner with little circumferential movement, simulation only considers a small sector containing only one fuel injector zone. The mesh is generated by software ICEM and the initial spacing of the boundary layer mesh has y+ values less than 1 to ensure the validity of using the SST model according to the former study in reference 21, and the whole domain nodes is about 1.5 million. Figure 5 shows hex meshes near the injector used for calculation. The flow conditions of this validation case are isolator inlet Mach number of 2.05, static pressure of 34100 Pa, static temperature of 1172 K, respectively. The volume fraction of oxygen is 0.26, the mole fraction of water vapor is 0.18, and the other is nitrogen. The hydrogen fuel is injected from the lower wall injection port only when chemical equivalence ratio is 0.35, and the total pressure of the fuel jet is 2.3 MPa. Both upper and lower wall injection ports are opened for chemical equivalence ratio1 and the corresponding total pressure of the fuel jet is 3.5 MPa.
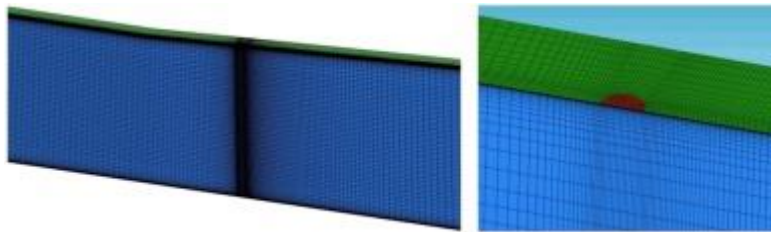

Fig. 5. The details of the structured mesh near the injector.

Figure 6 gives the comparison of experimental data [25] and present simulation results. For chemical equivalence ratio 0.35(see Figure 6(a)), it can be seen that the shock positions are predicted well in agreement with the experimental data although there is still a slight difference in the pressure peak locations. For chemical equivalence ratio 1.0 (see Figure 6(b)), simulation results agree perfectly well with the experimental data. These two simulation cases indicate that the SST turbulence model and EDM combustion model are suitable for obtaining the characteristics of high-speed reacting flow [27], which can be used in the primary design of scramjet engines.
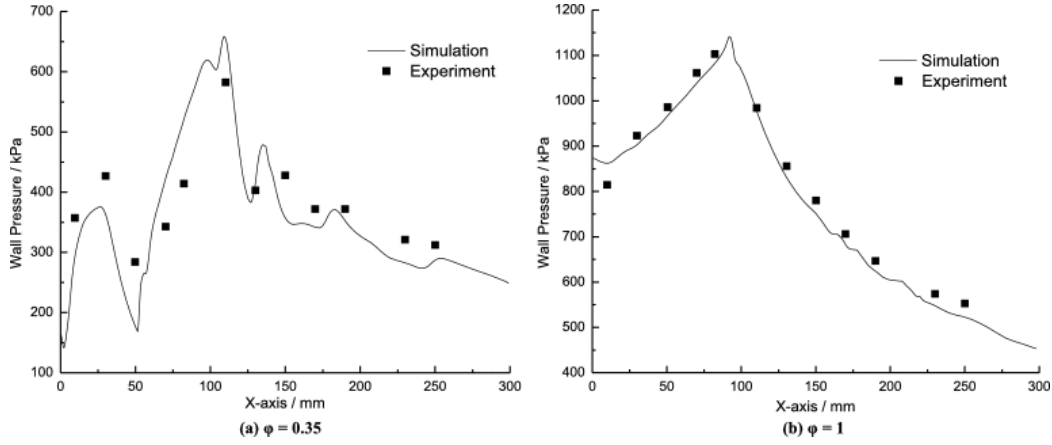
Fig. 6. The wall pressure distributions compared between simulation and experiment results

3. **Combustor Simulation and Discussion**

3.1. Boundary Layer Thickness Effect

The basic combustor model is an expanded circular duct with an entrance radius of 23.7 mm and an exit radius of 30.7 mm, and its length is 300 mm, as showed in Figure 7. Eight square hydrogen injectors (2mm×2mm) are evenly distributed around the circumferential direction at the entrance of combustor, before which there is an isolator of 300 mm long constant cross section area. As the geometric model is symmetrical, computational domain only takes 1/16 of the entire physical model, as showed in Figure 7.
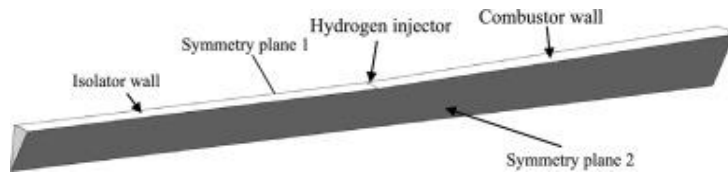
Fig. 7. Sketch of the computational domain

As the combustor is located in the middle of the engine, it is important to take the boundary layer thickness effect into account while simulating the combustion of hydrogen in combustor. In order to investigate the influence of airstream boundary layer thickness on combustion, a total of four different airstream boundary layer thickness conditions were simulated. In simulation, the boundary layer velocity profile was defined as below:

$$u = \begin{cases} U_e \left(\dfrac{y}{\delta} \right)^{\frac{1}{7}} & y < \delta \\ U_e & y \geq \delta \end{cases} \qquad (1)$$

Where δ is the pre-defined boundary layer thickness, Ue is the edge velocity of mainstream flow, y is the distance from the wall. The static pressure along the wall normal direction within the boundary

layer is assumed to be identical to that of the mainstream, and the static temperature was defined as below:

$$T_s = T_w + \left(T_{aw} - T_w\right)\frac{u}{U_e} - \frac{\gamma-1}{2}\cdot\sqrt{Pr}\cdot T_e\cdot M^2\left(\frac{u}{U_e}\right)^2 \qquad (2)$$

Where total temperature $T_{aw} = \left(1 + \frac{\gamma-1}{2}\cdot\sqrt{Pr}\cdot M^2\right)$, Tw is the wall temperature, γ is the ratio of specific heats, Pr is the Prandtl number, Te is the temperature of the mainstream, M is the Mach number of the mainstream.

The above two equations can be used to define all the parameters of the inlet boundary condition, four different boundary layer thicknesses with δ=0mm, 1mm, 2mm, 3mm, respectively were chosen as inlet boundary conditions, they were defined as cases 1 - 4 accordingly to be discussed below.

Figure 8 depicts Mach number contours in symmetry plane 1. Considering the entire flow field of isolator and combustor has a total length of 600 mm, the flow fields are generally similar except for the shock train part. Thus contours shown here were extracted portion of the whole domain with corresponding x-coordinate from −300 mm to 70 mm; with superimposed 0.01 isolines of the mass fraction of hydrogen in gray color as seen in Figure 8. It was clear that the location of the first shock moved forward gradually with the increasing of boundary layer thickness. It will be noticed that the thicker boundary layer is more easily to interact with adverse pressure gradient and result in flow separation along with formation of oblique shock train, thus in the condition of constant back pressure, the first shock tends to move forward as the boundary layer becomes thicker. In addition, different adverse back pressure here promoted this phenomenon.
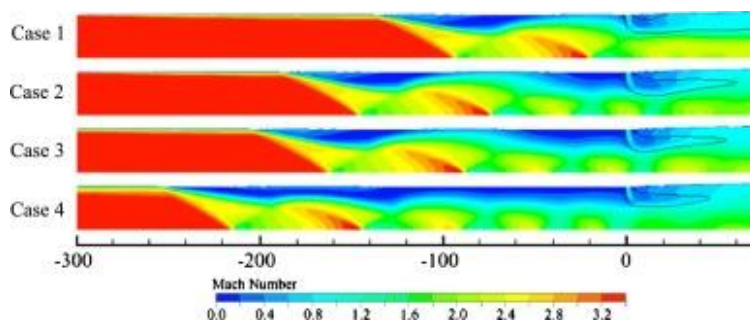

Fig. 8. Mach number contours in symmetry plane 1 of case 1 to case 4

Figure 9 gives the comparison of the stream wise wall pressure distributions of different cases. The computational results show that the thicker boundary layer the higher pressure peak values, which mean the thickening of the boundary layer can also cause the increase of the combustion back pressure. From the isolines of the mass fraction of hydrogen in Figure 8, it could be found that hydrogen tends to be consumed rapidly in those cases with a thicker boundary layer, because the low velocity zone near the nozzle will become large. Since hydrogen is injected from the wall, boundary layer thickness at the point of injection plays an important role in the combustion of fuel:

thicker boundary layer means relatively larger subsonic region and more hot air available to mix with fuel, both of which could promote combustion progress.
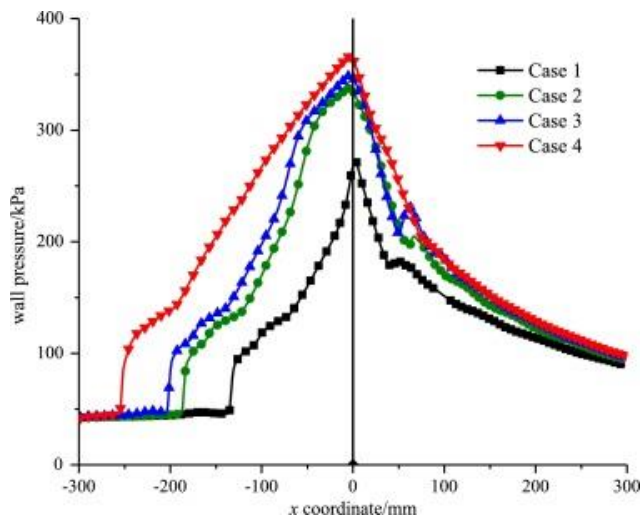

Fig. 9. Wall pressure distribution of case 1 to case 4

The combustion efficiency is calculated by the following method:

$$\eta = \frac{m_{burned}}{m_{total}}$$

(3)

Where m_{burned} represents the mass of hydrogen that has been totally burned in the combustor, m_{total} is the initial total mass of hydrogen that has been injected into the combustor. Table 1 summarizes the combustion efficiency of case 1 to case 4. From table 1 we can also confirms the tendency that has been mentioned above: thicker boundary layer corresponds with higher combustion efficiency. As hydrogen burns faster, back pressure of the isolator increases, making the shock train move upstream forward towards the inlet.

Table 1. Combustion efficiency of case1 to case 4

	η
Case 1	90.7%
Case 2	98.2%
Case 3	99.4%
Case 4	99.7%

3.2. Bleeding slot

To prevent the engine from 'unstart', one must ensure that the initial wave of the shock train does not propagate upstream into the inlet. Computational results show that bleed slots can be used to improve the isolator performance in pushing the shock train downstream. In the work described hereby, numerical simulations are performed to study the effect of bleed slot location on the shock train. According to a reference paper [26], oblique bleed slot could help to reduce the air mass flow loss, and the bleed slot here is designed as 2mm wide and 45° inclined, encircling the circumference of the isolator. The geometrical relations between the bleed slot and the isolator/combustor are shown in Figure 10, three different distances between the bleed slot and the combustor with x=10 mm, 50 mm, 100 mm are simulated, and they are defined as cases 5 - 7 separately. The inlet boundary layer thicknesses δ=3 mm, the exit bleed pressure of 2930 Pa are used respectively, and the other boundary conditions are the same as those of Case 4, 1/16 of the full geometry is taken as the computational model, the same as that seen in Figure 7.
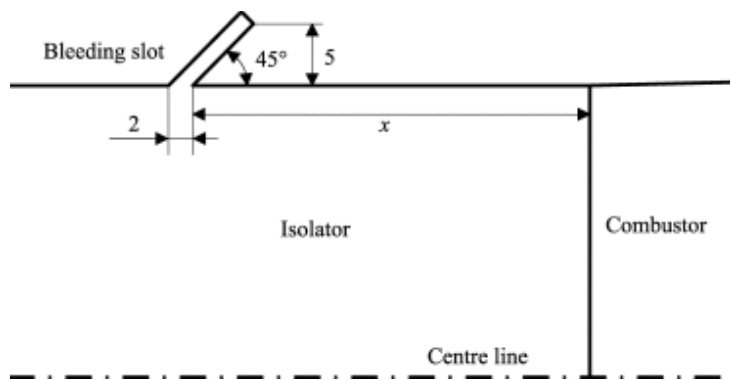

Fig. 10. Sketch of the geometrical relationship between the bleeding slot and the combustor

Figure 11 displays Mach number contours in symmetry plane 1, and the result of Case 4 without bleeding is used as a reference. Same as that showed in Figure 8, contours are extracted portion of the computational domain with corresponding x coordinate from -300mm to 70mm.
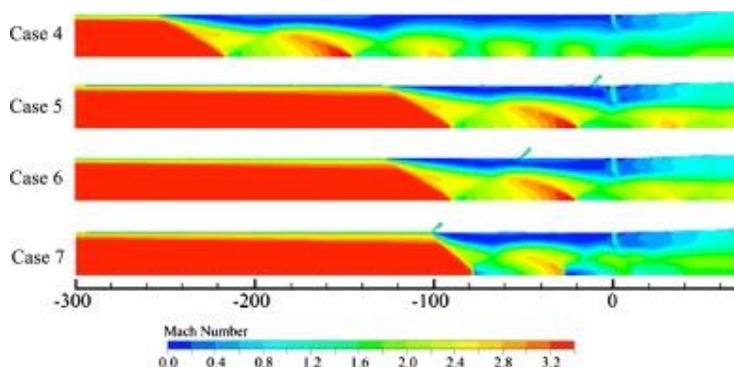

Fig. 11. Mach number contours in symmetry plane 1 of case 4 to case 7

By comparing with that of Case 4, other Cases 5-7 with the bleed slot pushed the shock train backward considerably, among which the flow fields of Case 5 and Case 6 are quite similar, and their bleed slots are both located in the subsonic region of the shock train. The shock train in Case 7 possesses the shortest length, with its first shock of intersecting with the local velocity vector (as showed in Figure 12), meaning the entire shock train spreading downstream of the bleed slot.
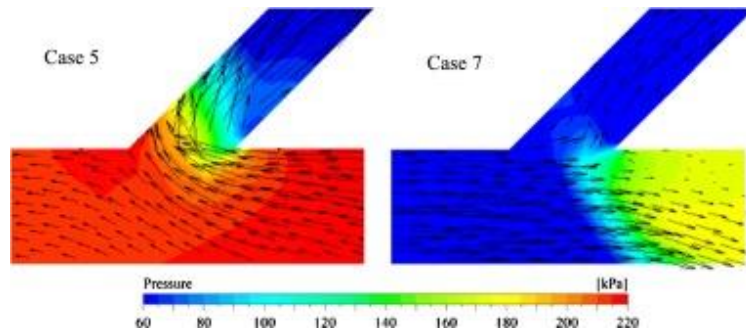

Fig. 12. Velocity vector and pressure near bleed slot compared of case 5 and case 7

Figure 12 shows the comparison of the local velocity vector in the vicinity of the bleed slot between Case 5 and Case 7. In Case 5, the flow direction near the bleed slot is reversed, which indicates the bleed slot is located inside the separation bubble, and the bleeding effect controlled the flow separation by weakening the reversed flow. While for Case 7, as the movement of the shock wave relies on its interaction with the boundary layer and also the adverse pressure gradient, the low momentum flow bleeding out of the boundary layer ahead of the shock wave would effectively restrain the shock train from moving further upstream.

Figure 13 depicts the centerline pressure distributions as a function of x coordinate. It can be found that in those cases with the bleed slots, the peak pressure of the first shock is higher than the case without bleeding. Particularly for Case 7, as also shown in Figure 11, its first shock wave has partly evolved into a normal shock wave in the vicinity of central line, which means higher pressure rise and thus more total pressure loss.
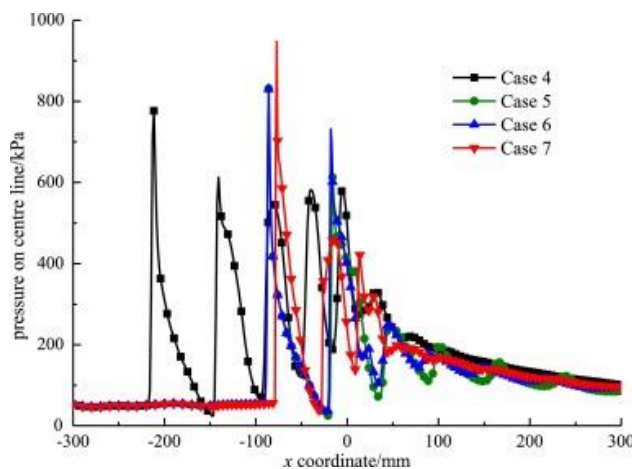

Fig. 13. Centre line pressure distribution of case 4 to case 7

Table 2 gives the performance parameters of four cases, among which Case 5 and Case 6 is very similar in terms of both the flow field and the performance parameters. The air mass loss of these two cases is higher than that of Case 7, because of the density of airstream increased significantly after the shock wave. Slight variations in combustion efficiency of all four cases indicate that the bleeding has limited effect on the combustion process. However, the total pressure recovery ratios of three bleeding cases are higher than that of non-bleeding reference Case 4. This is mainly because of the difference on the shock train: for Cases 5–7, there is a stronger first shock wave but the number of shock wave is only 2 or 3, while for Case 4, its first shock is only slightly weaker but the number of shock wave is 5, which will cause more total pressure loss.

Table 2. Performance parameters of case 4 to case 7

	x/mm	air mass loss	combustion efficiency η	total pressure recovery σ
Case 4			99.7%	0.19
Case 5	10	3.9%	96.7%	0.30
Case 6	50	3.6%	97.2%	0.30
Case 7	100	2.0%	98.4%	0.24

3.3. Interval of hydrogen injectors

Another method to prevent the shock train from propagating upstream is to decrease the back pressure. By diverging hydrogen injectors along the axial direction, it can relieve the concentration of the heat release at the entrance of the combustor. Thus, a model concept is proposed here by increasing the axial distance between each hydrogen injector and in the meantime keeping the bilateral symmetry, as showed in Figure 14. Four different model variants with a long interval of Δx=5 mm, 10 mm, 20 mm, 50 mm, respectively are considered and simulations are defined as Cases 8- 11 separately. Inlet boundary layer thicknesses δ=0 mm is chosen, and other boundary conditions are consistent with that of Case 1,with 1/2 of the full geometry is taken as the computational domain.
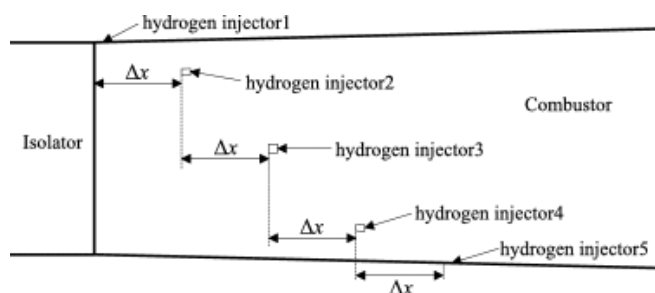

Fig. 14. Diagrammatic sketch of geometrical relationship between injectors and the combustor

Figure 15 displays Mach number contours in the symmetry plane of an extracted portion corresponding to x-coordinate of −165 mm to 300 mm. It can be seen that as the axial length between the hydrogen injectors increases, the flow field tends to become asymmetric.
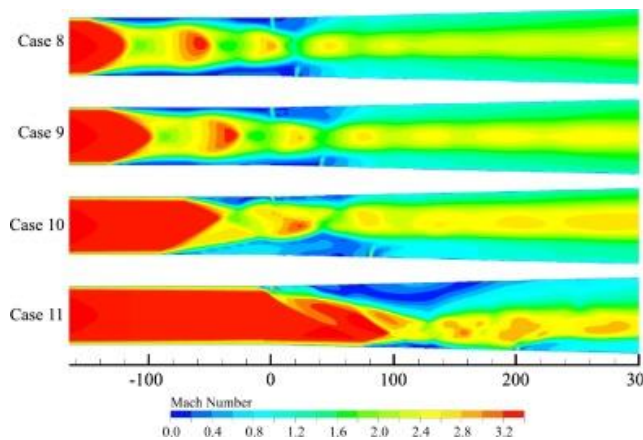

Fig. 15. Mach number contours in symmetry planes of case 8 to case 11

Taking Case 11 for instance, Figure 16 gives the Mach number contours on uniformly spaced successive cross-sections of, in which the black blocks represent the hydrogen injector location. It is found that as high speed hydrogen jet interacts with the main airstream, the low speed zones formed downstream of each injector, among which low speed zones formed by the injectors 4 and 5 are observed flow separation close to the wall. While low speed zones formed by the injectors 1, 2, 3 finally merge together into a large zone which almost occupies the upper part of the entire flow field and hence pushed the main airstream aside. Another characteristic feature concluded from Figure 16 is that the shock train moved backward (i.e. downstream) as the axial length interval of the hydrogen injector increases. This is mainly due to the different combustion processes occurred in the combustor.
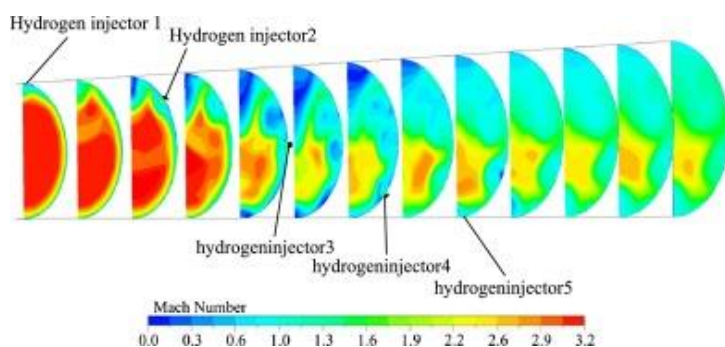

Fig. 16. Mach number contours on cross-sections in the combustor of case 11

Figure 17 gives the consumption rate of hydrogen and Figure 18 illustrates the mass-weighted average pressure along the axial direction in the combustor. In Figure 17, the results of Cases 8, 9, and 10 are quite similar in terms of the general trends, i.e. they rise rapidly during the initial stage and flatten out in the final stage. At the position of x=100, i.e.1/3 of the combustor, there are 83.0%,

79.5%, 61.9% of hydrogen consumed in Cases 8, 9 and 10 separately, indicating that the heat release will mainly concentrate in the fore part of the combustor in these three cases. While for Case 11, the result appears to be distinctly different from other three cases, i.e.it climbs steadily throughout the entire combustor, which means hydrogen is more evenly consumed along the axial direction and the heat release is no longer concentrated in anywhere in the combustor. These observed combustion features could be easily reflected in the pressure distributions, as showed in Figure 18. The pressure peak of Case 11 is much lower and appeared further downstream in the combustor than that of other cases. This is probably the reason why the shock train in Case 11 has the least effect on the flow field of the isolator.
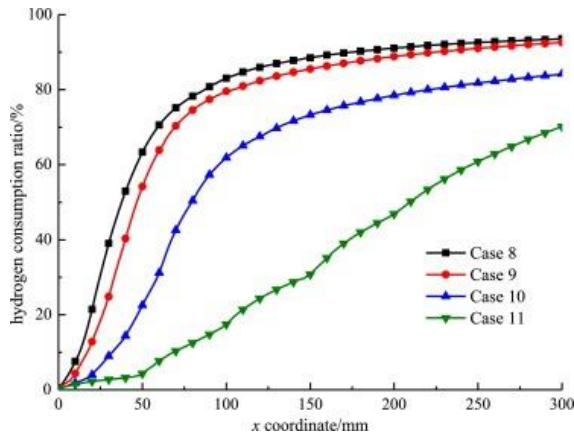

Fig. 17. Consumption rate of hydrogen along the axial direction in combustors of case 8 to case 11
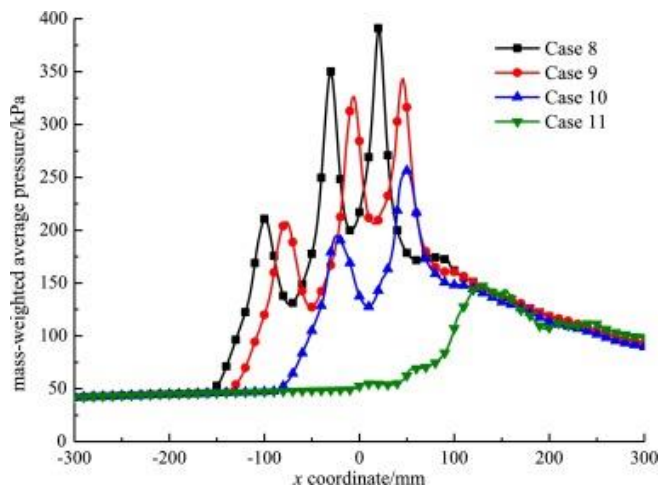

Fig. 18. Mass-weighted average pressure along the axial direction in combustors of case 8 to case 11

Discussions above have concluded that the divergence of the hydrogen injectors could decrease the back pressure. However, there still have been some disadvantages for this method, e.g. at x=300 mm the combustion efficiency (as saw in Figure16) of Case 8 is about 93.6% and for Case 11, it drops to merely 70.2%. This is mainly due to the re-location of the hydrogen injectors in the axial direction that would make some injectors being in the rearward of the combustor, and it is inevitable that the combustion efficiency drops down because some portions of hydrogen may escape from the combustor, thus having little contribution to the combustion progress.

4. **The Whole Engine Simulation and Discussion**

4.1. Realistic model with inlet

In order to assess the impacts of those factors described above in the real conditions, a new combustor model with inlet and isolator was generated: i.e. the inlet was based on a truncated Busemann inlet. After streamline tracing, lip retreating and boundary layer correction, its final appearance is shown in Figure 19. The length of the isolator is 100 mm, and the axial interval of hydrogen injectors is 50mm. In order to enhance the combustion efficiency, a cavity close to the exit of the combustor is used and its geometry is depicted in Figure 20. The size of the cavity is 10 mm deep and 30 mm wide, with the slope angle of the back wall of 45 degrees. The entire computational domain is shown in Figure 21. Free stream conditions are Mach number of 6, static temperature 220.7 K, static pressure 2930.7 Pa, respectively and the hydrogen is injected in acoustic sonic speed with static temperature at 800 K and static pressure 0.48 MPa, resulting an equivalence ratio of 0.5.

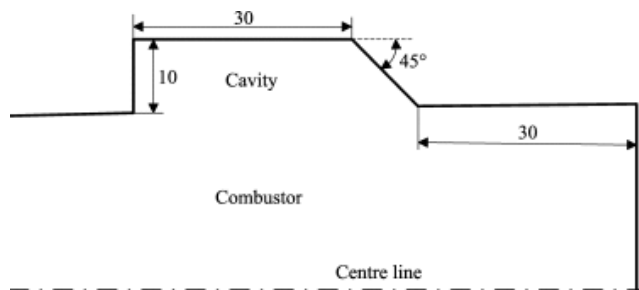Fig. 19. The inlet model for the scramjet

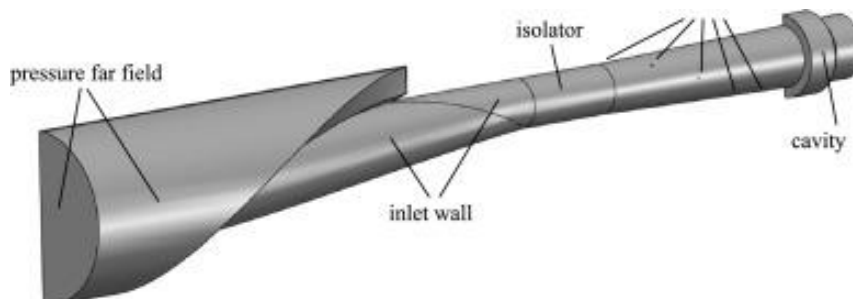Fig. 20. The cavity geometry and the location in the combustor

Fig. 21. The whole computational domain of the model with Busemann inlet

Figure 22 shows Mach number contours of the isolator and the combustor in the symmetry plane, corresponding to x-coordinate from −100 mm to 300 mm. Similar to that seen in the Case 11, the back pressure of combustion has little influence on the flow field of isolator.
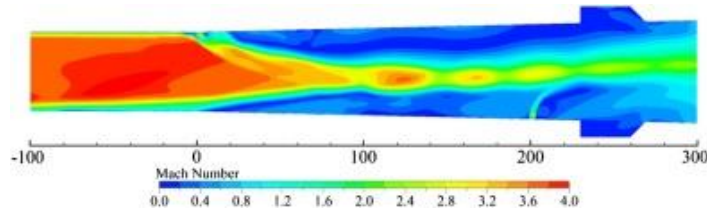

Fig. 22. Mach number contours in symmetry plane of the whole computational domain

Figure 23 gives Mach number contours on uniformly spaced successive cross-sections in the combustor. The Mach number contour (as seen in Figure 23(a)) differs from that observed in Figure 16, i.e. the large low speed zone not only appears in the upper part but also in the lower part of the combustor. This is probably due to the shape of the inlet, as its bottom wall is much longer than the upper wall, resulting in the boundary layer thickness increases more significantly along the bottom wall than that of the top wall at the exit of the inlet and the flow field of downstream, which inherits this characteristic. For the combustor, as its boundary layer near the bottom wall is the thickest, enhanced adverse pressure gradient would naturally lead to flow separation and low speed zone at the lower part. Considering the low speed zone near the top wall caused by the hydrogen injection, the flow field shown in Figure 23(a) reveals that the high speed zone of the main airstream is narrowed down to an area near the center line that is much smaller than that of the sectional area. The hydrogen mole fraction contours (as seen in Figure 23(b)) shows that there are two high concentration regions of hydrogen at the exit of the combustor, and by tracing back from upstream it could be found that hydrogen from injector 3 mainly contributes to high concentration region① and the hydrogen from injectors 4 and 5 mainly contribute to high concentration region②. In other words, the injectors in the rearward of the combustor are the principal causes of the combustion efficiency descend. From Figure 23(c), it is clear that the high temperature mainly appears near the wall surface and it is consistent to the low speed zone seen in Figure 23(a), which indicates low speed is the key factor that propitious to the combustion.

(a) Mach number contour

(b) Hydrogen mole fraction contour
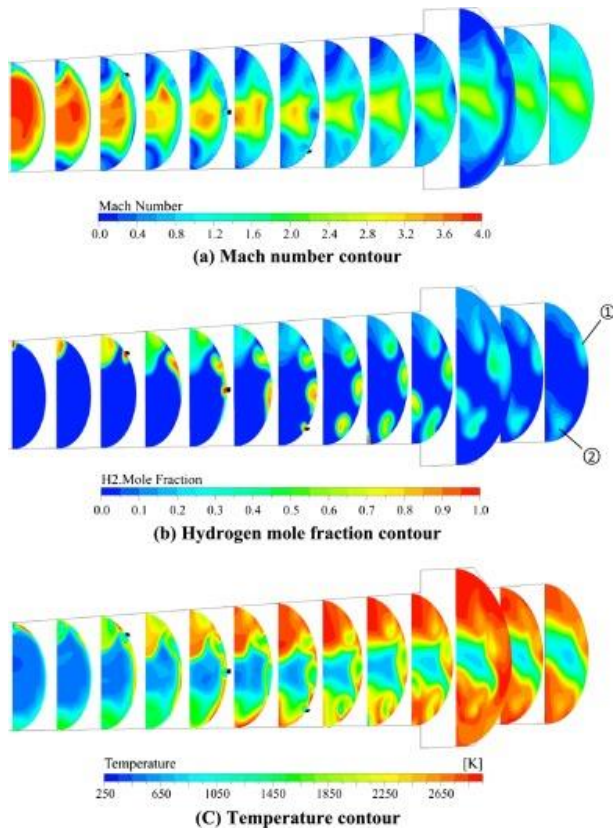
(C) Temperature contour

Fig. 23. Contours on cross-sections in the combustor of the whole computational domain

4.2. Effect of chemical equivalence ratio

The effect of chemical equivalence ratio on hydrogen static pressure is studied. The ratio is increased from 0.5 to 0.7 by a step size of 0.1, defined as Cases 12–14 separately. When the equivalence ratio reaches 0.8, the inlet is found unstated, this ratio higher than 0.7 is not considered. Figure 24 depicts Mach number contours of the combustor, the isolator and the internal contraction section of the inlet in the symmetry plane, corresponding to x-coordinate from –255 mm to 300 mm. It is found that the flow fields of these cases are quite similar, and the main difference lies in the flow separation near the bottom wall to which it moves upstream along with the increase of the equivalence ratio.
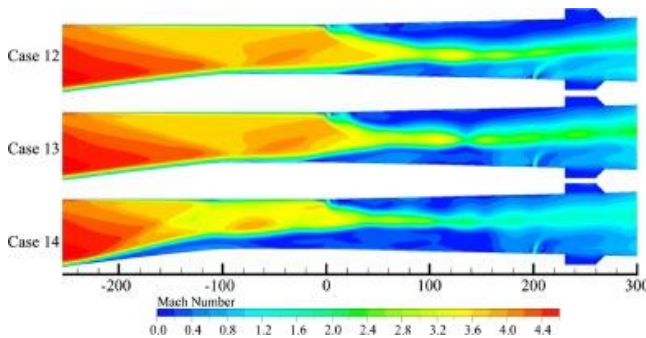

Fig. 24. Mach number contours in symmetry plane of case 12 to case 14

Figure 25 depicts the mass-weighted average pressure along the axial direction, and it is found that the high amplitude pressure fluctuations appear only in the combustor (i.e. x=0–300 mm), while the pressure variation in the isolator (−100 – 0 mm) seems to be placid. Under this circumstance, it is not the shock train but merely the flow separation caused by the adverse pressure gradient that moves upstream. For the inlet, the flow separation near the bottom wall means the shrink of flow area and thus the increase of the contraction ratio. When the back pressure in the combustor is high enough, the flow separation in the inlet would plug a sufficiently large area and makes the flow field of the inlet becoming 'unstart' finally.
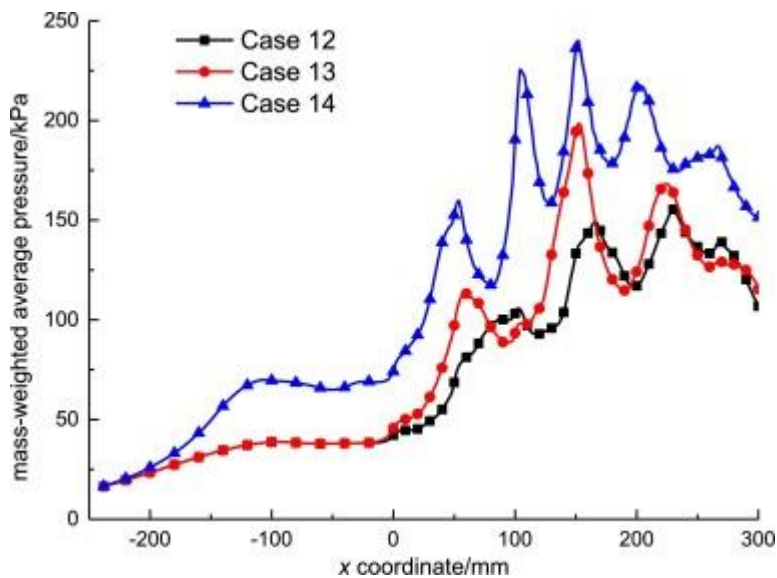

Fig. 25. Mass-weighted average pressure of case 12 to case 14

4.3. Model with the bleeding slot

In addition to the chemical equivalence ratio, a bleed slot with 10mm wide and 45° inclination is located in the isolator 5mm from the exit of the inlet. The exit pressure of the bleed is 2930.7 Pa. The free stream conditions are the same as that of Case 12. Because the air mass loss due to bleeding is unknown at first, the chemical equivalence ratio calculated here is based on the flow captured at the inlet, i.e. ф=0.8−1 is defined in Cases 15–17 separately.

Figure 26 gives Mach number contours of the isolator and the combustor in the symmetry plane. With bleeding, the low momentum fluids in the boundary layer and the flow fields are slightly different from those cases without bleeding: e.g. the flow separation near the top wall does not developed into a large low speed zone and the flow separation near the bottom wall could not stride over the slot in all cases. Both of them are results of decreasing boundary layer thickness due to the bleed slot.
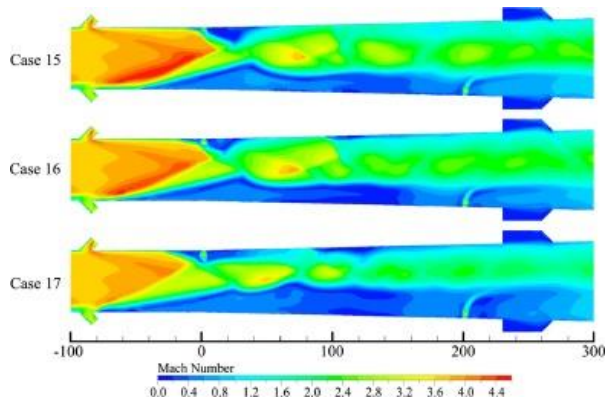
Fig. 26. Mach number contours in symmetry plane of case 15 to case 17

Table 3 summarizes the parameters of two models used in all cases. It can be concluded that in a specific model, the combustion efficiency has less significant change while the equivalence ratio varies. Compared with the initial model, the models with bleeding have lower combustion efficiency. Of Mach number contours seen in Figure 24 and Figure 26, it is noted that the low speed zone in the bleeding model is smaller than that in the initial model. Thus, the low speed zone would be a key factor that propitious to the combustion, as a result a drop occurred in the combustion efficiency is understandable. The air mass loss of the bleeding model remains almost unchanged for different equivalence ratios tested, which is mainly attributed to the relatively stable position of the first shock wave downstream the bleeding slot.

Table 3. Performance parameters of two different models

	equivalence ratio φ	combustion efficiency η	total pressure recovery σ	air mass loss
Case 12	0.5	74.8%	0.15	
Case 13	0.6	72.1%	0.14	
Case 14	0.7	75.8%	0.084	
Case 15	0.8	63.5%	0.12	4.92%
Case 16	0.9	66.8%	0.10	4.93%
Case 17	1.0	65.7%	0.084	4.93%

5. Conclusions

Different dominant factors which influence the shock train in a scramjet engine have been investigated via numerical simulations, and the critical simulation model has been validated with published experimental results. The numerical results are realistic and applicable in practice because

that the investigated scramjet engine model assembles the practical geometry with an axisymmetric isolator and combustor with staged wall injection and slot suction, and that the investigated working conditions are chosen to fit the typical operational conditions. From a comprehensive aspect of the scramjet engine design, several suggestions to control the air-breathing conditions and to enhance the combustion performance can be drawn from the control of the shock train.

1) The increase of the boundary layer at the entrance of the combustor pushes the shock train upstream, so it tends to cause the 'unstart' in the inlet of the engine, although it increases the combustion efficiency. Those two consequences need to be balanced, so the suggestion for the engine design is to maintain the boundary layer thickness at an appropriate value.

2) The increase of the back pressure in combustion would cause flow separation near the bottom wall to move upstream towards the inlet of the engine, which is equivalent to the increase of the contraction ratio. A final consequence of the phenomena above is the 'unstart' of inlet, so the suggestion for the engine design is to maintain the back pressure or the contraction ratio within a relatively low value.

3) The introduction of bleeding slots can effectively move the first shock wave backward, reduce the total pressure loss, and raise the upper limit of chemical equivalence ratio, but it inevitably decreases the combustion efficiency drop. In applications, this controlling method by bleeding slots requires further optimization to balance those opposite effects.

4) The introduction of staged wall injection of hydrogen in the combustor promotes the combustion, and increasing the axial distance between adjacent hydrogen injectors reduces the combustion back pressure. It relieves the burden of the isolator. However, the flow field in the combustor would become asymmetric and the combustion efficiency would drop significantly. Therefore, this controlling method by hydrogen injection also requires further optimization in applications.

References

[1] Curran E. T. Scramjet Engines: The First Forty Years. Journal of Propulsion and Power, Vol. 17, No. 6, 2001, pp. 1138-1148.

[2] Yakar A. B. and Hanson R. K. Cavity Flame-Holders for Ignition and Flame Stabilization in Scramjets: An Overview. Journal of Propulsion and Power, 2001, Vol. 17, No. 4, pp. 869-877.

[3] Zhang X. Compressible cavity flow of oscillation due to shear layer instabilities and pressure feedback. AIAA Journal, 1995, Vol. 33, No. 8, pp. 1404–1411.

[4] Gruber M.R., Baurle R.A., Mathu T. r, Hsu K.-Y. Fundamental studies of cavity-based flame holder concepts for supersonic combustors. Journal of Propulsion and Power, 2001, Vol. 17, No. 1, pp. 146–153.

[5] Rasmussen C. C., Driscoll J. F., Hsu K. Y. and etc. Stability Limits of Cavity-Stabilized Flames in Supersonic Flow. Proceedings of the Combustion Institute, 2005, Vol. 30, pp. 2825-2833,

[6] Liu J., Tam C., Lu T. and Law C. K. Simulations of Cavity-stabilized Flames in Supersonic Flows Using Reduced Chemical Kinetic Mechanisms. 42nd AIAA/ASME/SAE/ASEE Joint Propulsion Conference & Exhibit, 2006, July9-12, Sacramento, California.

[7] Barber T. A., Maicke B. A. andMajdalani J. Current State of High Speed Propulsion: Gaps, Obstacles, and Technological Challenges in Hypersonic Applications. 45th AIAA/ASME/SAE/ASEE Joint Propulsion Conference & Exhibit, 2009, August 2–5, Denver, NV.

[8] Waltrup P J, Billig F S. Prediction of precombustion wall pressure distributions in scramjet engines. Spacecraft Rockets, 1973, Vol. 10, No.9, pp. 620-622.

[9] Holland S. D. Wind-Tunnel Blockage and Actuation Systems Test of a Two Dimensional Scramjet Inlet Unstart Model at Mach 6. NASATM-109152.1994.

[10] Daren Y., Chang J., Bao W., and Xie Z. Optimal Classification Criterions of Hypersonic Inlet Start/Unstart. Journal of Propulsion and Power, 2007, Vol. 23, No. 2, pp. 310-316.

[11] Wang Y., Wang Z., Liang J., and Fan X. Investigation on Hypersonic Inlet Starting Process in Continuous Free jet Wind Tunnel. Journal of Propulsion and Power, 2014, Vol. 30, No. 6, pp. 1721-1726.

[12] Zinnecker A M. Modeling for Control Design of an Axisymmetric Scramjet Engine Isolator[D]. The Ohio State University, 2012.

[13] Wagner J L, Yuceil K B, Clemens N T. Velocimetry measurements of unstart of an inlet-isolator model in Mach 5 flow[J]. AIAA journal, 2010, 48(9): 1875-1888.

[14] Wagner J L, Yuceil K B, Valdivia A, et al. Experimental investigation of unstart in an inlet/isolator model in Mach 5 flow[J]. AIAA journal, 2009, 47(6): 1528-1542.

[15] Do H, Im S, Mungal M G, et al. Visualizing supersonic inlet duct unstart using planar laser Rayleigh scattering[J]. Experiments in fluids, 2011, 50(6): 1651-1657.

[16] Fei Xing, Yue Huang, Xiaoyuan Fang, Yufeng Yao. Numerical Investigation on Two Streamline-Traced Busemann Inlet-Isolators. 54th AIAA Aerospace Sciences Meeting 4-8 January 2016, San Diego, California.

[17] Billig F. S., Baurle R. A., Tam C. J. Design and analysis of streamline traced hypersonic inlets. 9th International Space Planes and Hypersonic Systems and Technologies Conference, 1-5 November, 1999, Norfolk, VA.

[18] Xiao Y. B., Yue L. J., Gong P., and Chang X. Y. Investigation on a truncated streamline-traced Busemann inlet. 15th AIAA International Space Planes and Hypersonic Systems and Technologies Conference, 28 April-1 May, 2008, Dayton, Ohio.

[19] O'Brien T. F., and Colville J. R. Analytical computation of leading edge truncation effects on inviscid Busemann inlet performance. Journal of Propulsion and Power, 2008, Vol. 24, No. 4, 655-661.

[20] Zhang H., Tan H. J., and Sun S., Characteristics of shock-train in a straight isolator with interference of incident shock waves and corner expansion waves. Acta Aeronoutica et Astronautica Sinica, 2010, Vol. 31, No. 9, pp. 1733-1739. (In Chinese)

[21] Xing, F. Yao, Y., and Zhang, S., "Numerical Simulation of Shock-Induced-Combustion in Three-Dimensional HyShot Scramjet Model," AIAA paper 2012-0945, 2012.

[22] Gounko Y. P. and Mazhul I. I., Gasdynamic design of a two-dimensional supersonic inlet with the increased flow rate factor. Thermophysics and Aeromechanics, 2012, Vol. 19, No. 3, pp. 363-379.

[23] Gounko Y. P. and Mazhul, I. I. Improvements in Modeling 90-Degree Bleed Holes for Supersonic Inlets. Journal of Propulsion and Power, 2012, Vol. 28, No. 4, pp. 773-781.

[24] Müller F., Schmitt, M., Wright, Y., and Boulouchos, K. Determination of Supersonic Inlet Boundaries of Gaseous Engines Based on Detailed RANS and LES Simulation. SAE International Journal of Engines, 2013, Vol. 6, No. 3, pp. 1532-1543.

[25] Zheng, Z.H. Massively Parallel Computing of Dual-Mode Scramjet Combustor and its Experimental Verification. Ph.D. Dissertation, Graduate School of National University of Defense Technology, Changsha, China, 2003.

[26] Cao X.B., Zhang K.Y., Gao L.J. Numerical investigation of a new short isolator bleed slots. Journal of Propulsion Technology, 2011, Vol. 32, No. 2, pp. 159-164. (In Chinese)

[27] Wang P., Chen M., Xing F., et al. CFD numerical simulation of Hyshot scramjet. Journal of Aerospace Power, 2014, Vol. 29, No. 5, pp. 1020-1028. (In Chinese)